

UNIGRAZ-UTP-14-07-97
hep-lat/9707011

Topological Charge and the Spectrum of the Fermion Matrix in Lattice-QED₂ *

C.R. Gattringer

Department of Physics and Astronomy,
University of British Columbia, Vancouver B.C., Canada

I. Hip and C.B. Lang

Institut für Theoretische Physik
Universität Graz, A-8010 Graz, Austria

Abstract

We investigate the interplay between topological charge and the spectrum of the fermion matrix in lattice-QED₂ using analytic methods and Monte Carlo simulations with dynamical fermions. A new theorem on the spectral decomposition of the fermion matrix establishes that its real eigenvalues (and corresponding eigenvectors) play a role similar to the zero eigenvalues (zero modes) of the Dirac operator in continuous background fields. Using numerical techniques we concentrate on studying the real part of the spectrum. These results provide new insights into the behaviour of physical quantities as a function of the topological charge. In particular we discuss fermion determinant, effective action and pseudoscalar densities.

PACS: 11.15.Ha, 11.10.Kk

Key words: Lattice field theory, topological charge, spectral decomposition, dynamical fermions, Schwinger model

* Supported by Fonds zur Förderung der Wissenschaftlichen Forschung in Österreich, Projects P11502-PHY and J01185-PHY.

1 Introduction

Topological concepts play a prominent role in our understanding of continuum gauge theories. An example of particular importance is the idea that for the true vacuum functional of QCD (θ -vacuum) gauge field configurations of all topological charges have to be taken into account in the path integral [1]. Such statements however are difficult to formulate in a mathematically precise way. The topological charge is a concept for classical, i.e. differentiable fields, since only those fields can be uniquely classified with respect to an integer topological charge. On the other hand differentiable configurations are of measure zero in the path integral for the gauge fields (see e.g. [2]).

When formulating gauge theories on the lattice the notion of a classical gauge field configuration gets lost. However, various definitions of a topological charge for lattice gauge fields have been proposed (see e.g. the review [3] and also [4] for an overview on more recent developments). Using such a prescription one can in principle assign a topological charge to every lattice configuration (up to so-called exceptional configurations which in the continuum limit do not contribute to the path integral). In a certain sense this makes the lattice approach very powerful for pursuing topological concepts since the path integral can indeed be decomposed into topological sectors whereas in the continuum formulation topological arguments are restricted to (non-contributing) classical configurations.

The working hypothesis, that every gauge field configuration contributing to the lattice path integral in the continuum limit can be assigned a topological charge, allows to decompose the lattice path integral into topological sectors. As discussed above, in the continuum this is only possible in a formal way. The topological decomposition of the *lattice* path integral is a conceptionally sound procedure and allows to address many interesting physical questions in a mathematically meaningful setting.

For classical gauge field configurations the Atiyah Singer Index Theorem [5] provides a powerful tool connecting the topological charge with the zero modes of the Dirac operator. However in the continuum path integral its value is reduced to formal or semi-classical arguments, since the classical configurations are of measure zero as remarked above.

On the lattice the situation is different. On one hand when approaching the continuum limit, every gauge field configuration contributing in the con-

tinuum limit can be assigned a topological charge. On the other hand we have no such thing as the Atiyah Singer Index Theorem on the lattice. However, in the literature several investigations [6] - [11] attempting to establish the Index Theorem on the lattice in a probabilistic sense can be found. If such a goal is achieved, together with the fact that the lattice path integral can be decomposed into topological sectors, this would allow to gain better insight into the behaviour of fermionic observables using the connection between topology and the spectrum of the fermion matrix.

In this article we study QED₂ on the lattice to demonstrate that a tight connection between topology and spectrum of the fermion matrix can be found and provides a powerful mathematical tool. Establishing this connection is a two step procedure. In a first step we use analytic arguments to understand general features of the spectrum of the fermion matrix. In particular we prove a new theorem on the chiral properties of the eigenvectors of the fermion matrix, which makes clear that only the real eigenvalues play a special role similar to zero eigenvalues (and zero modes) of the continuum Dirac operator. These analytic results can be generalized to the 4-dimensional Wilson-Dirac operator [12].

Once the real eigenvalues are identified as being the trace of the topological charge in the spectrum, in a second step we concentrate on analyzing their properties using numerical methods. Tracing only the real eigenvalues is a much simpler task than investigating all eigenvalues of the fermion matrix. For sufficiently large β we establish results on size and distribution of the real eigenvalues and show that their number is related to the topological charge computed with the geometric definition [13]. In a final section we make use of these results and use them to discuss the behaviour of the fermion determinant, the effective action and the pseudoscalar densities.

The model under consideration (QED₂) resembles many features of 4-dimensional gauge theories such as QCD. In particular U(1) gauge theory in 2 dimensions allows for classical topologically nontrivial configurations ('vortices') which play the role of the instantons of 4D Yang-Mills theory. QED₂ has an anomaly which is related to the mass generation of the pseudoscalar singlet as in QCD. Thus the lattice version of this low dimensional model is an interesting candidate when exploring the role of topology in lattice models. Moreover for the continuum model there exists a limit which can

be solved analytically. When setting the fermion masses to zero, the model reduces to the Schwinger model [14] for two species of fermions. This allows to check the lattice simulations and to gain intuition from the analytic result. For the case of massive fermions semiclassical results [15] and expansions in the bare mass are available [16].

The article is organized as follows: Sec. 2 contains a short discussion of the model, the details of the simulation as well as definitions and theorems for the topological charge in the continuum and on the lattice. In Sec. 3 we develop the analytic results for the spectral decomposition of the fermion matrix and in Sec. 4 we analyze the spectrum using numerical techniques. Finally in Sec. 5 we discuss the applications outlined above. The article ends with a discussion (Sec. 6).

2 Setting

This section prepares the ground for the program outlined in the introduction. We formulate the lattice model, present technical details of the simulation and discuss the definitions and results for the topological charge in the continuum as well as on the lattice.

2.1 QED₂ on the Lattice

We work on a two dimensional lattice Λ with volume L^2 . Lattice sites are denoted as $x = (x_1, x_2)$ with $x_i = 1, 2, \dots, L$. The lattice spacing is set equal to 1. The gauge fields are group elements $U_\nu(x) \in \text{U}(1)$ assigned to the links between nearest neighbours $x, x + \hat{\nu}$ and their action is given by

$$S_g = \beta \sum_{x \in \Lambda} \left[1 - \text{Re } U_P(x) \right], \quad (1)$$

where the plaquette element is defined as

$$U_P(x) = U_1(x) U_2(x + \hat{1}) \overline{U_1(x + \hat{2})} \overline{U_2(x)}. \quad (2)$$

The gauge fields obey periodic boundary conditions $U_\nu(L+1, x_2) = U_\nu(1, x_2)$, $U_\nu(x_1, L+1) = U_\nu(x_1, 1)$. The fermion action is the bilinear form (in matrix notation)

$$S_f = -\bar{\psi} M \psi,$$

where the (implicit) summation is over lattice points and spinor indices - the above mentioned two flavors come about through squaring the fermion matrix (see below). We write the fermion matrix as

$$M = 1 - \kappa Q , \quad (3)$$

where the hopping matrix Q is defined as (spinor indices still suppressed)

$$\begin{aligned} Q(x, y) &= \sum_{\nu=1,2} Q_{\nu}(x, y) , \\ Q_{\nu}(x, y) &= (1 + \gamma_{\nu})U_{\nu}(x - \hat{\nu})\Delta_{x-\hat{\nu},y} + (1 - \gamma_{\nu})\overline{U_{\nu}(x)}\Delta_{x+\hat{\nu},y} . \end{aligned} \quad (4)$$

β is related to the bare coupling constant e via $\beta = 1/e^2$ and the hopping parameter κ to the bare mass m through $\kappa = (2m + 4)^{-1}$. The matrices γ_{ν} are chosen as the Pauli matrices $\gamma_{\nu} = \sigma_{\nu}$, $\nu = 1, 2, 3$. The fermions obey mixed boundary conditions, i.e. periodic in $\hat{1}$ -direction and antiperiodic in $\hat{2}$ -direction. This is taken into account by the mixed periodic Kronecker delta defined as

$$\begin{aligned} \Delta_{x-\hat{1},y} &= \delta_{x_2,y_2} \left[\delta_{x_1,1}\delta_{y_1,L} + \delta_{x_1,2}\delta_{y_1,1} + \dots + \delta_{x_1,L}\delta_{y_1,L-1} \right] , \\ \Delta_{x+\hat{1},y} &= \delta_{x_2,y_2} \left[\delta_{x_1,1}\delta_{y_1,2} + \dots + \delta_{x_1,L-1}\delta_{y_1,L} + \delta_{x_1,L}\delta_{y_1,1} \right] , \\ \Delta_{x-\hat{2},y} &= \delta_{x_1,y_1} \left[-\delta_{x_2,1}\delta_{y_2,L} + \delta_{x_2,2}\delta_{y_2,1} + \dots + \delta_{x_2,L}\delta_{y_2,L-1} \right] , \\ \Delta_{x+\hat{2},y} &= \delta_{x_1,y_1} \left[\delta_{x_2,1}\delta_{y_2,2} + \dots + \delta_{x_2,L-1}\delta_{y_2,L} - \delta_{x_2,L}\delta_{y_2,1} \right] . \end{aligned} \quad (5)$$

Obviously $\Delta_{y-\hat{\nu},x} = \Delta_{x+\hat{\nu},y}$. We are rather explicit here, since the analytic results for the spectrum of the fermion matrix in a fixed background configuration depend on the boundary conditions and also change whether L is even or odd. The latter dependence can be discussed conveniently using $\Delta_{x\pm\hat{\nu},y}$. It has to be remarked, that when actually integrating over all gauge configurations the boundary conditions for the fermions are irrelevant for this model, since gauge group $U(1)$ contains also -1 . For a given gauge field configuration there is a partner differing just in the boundary links by a factor -1 . The operators resulting from the Grassmann integral over fermion thus are averaged over these configurations.

2.2 Technical details of the simulation

We use lattices of size L^2 with L between 4 and 16. In the Monte Carlo simulation the fermions were considered with the hybrid Monte Carlo method [17]. In order to ensure positivity of the fermion determinant measure we had to introduce a second species of fermions. We stress that we squared the fermion determinant only for generating Monte Carlo configurations, whereas below we analyze the spectrum and other properties of M as defined in (3) and (4) (not M^2). In the HMC method we used trajectories with 10 steps and a step size adjusted such that the acceptance rate in the Monte Carlo step was 0.8 in the average.

For the inversion of the fermion determinant even-odd preconditioning was used, together with the BiCG γ_5 (actually BiCG σ_3) algorithm [18]. This proved to be efficient for most configurations. Whenever we found slow convergence (so-called “unstable configurations”, also often called exceptional, in contradistinction to the notation for configurations without definite topological charge to be discussed later) we switched the inverter and used BiCGStab (biconjugate gradient stabilized, cf. e.g. [19]) without preconditioning, which seemed to be the most reliable (although not most efficient) method.

In general we do not observe any abundance of unstable configurations close to κ_{crit} but actually only very few ($\mathcal{O}(0.1\%)$), which then were successfully inverted by BiCGStab. In fact, we even can work at values above the presumed κ_{crit} without noticeable problems.

In the computations below, we simulate the model at the values of κ given in Table 1. These numbers have been chosen from preliminary results on $\kappa_{crit}(\beta)$, that have been determined with help of restoration of PCAC along the lines of [20]. (The final results and their size dependence are discussed in [21]. It turns out that the κ -values of Table 1 are slightly (typically 0.001) below the critical values determined in [21].) These values are consistent with the behaviour of other observables like the chiral susceptibility. We used these κ -values for all lattice sizes. As will be discussed below, our results are only weakly dependent on the precise value of the hopping parameter. The eigenvalues of the hopping matrix Q were determined by general purpose routines for non-hermitian matrices. Since the configurations are comparatively small, direct determination of all eigenvalues and eigenvectors was possible throughout.

β	0.1	0.5	1.0	1.5	2.0	3.0	4.0	5.0
κ	0.332	0.314	0.296	0.286	0.276	0.267	0.262	0.260

Table 1: Values of κ for different β .

2.3 Topological charge in the continuum and on the lattice

In this subsection we discuss the topological charge in the continuum and its geometric definition on the lattice. We state the Atiyah-Singer Index Theorem and the less known Vanishing Theorem which holds for QED₂.

We start with collecting some results for QED₂ in the continuum which can be found in the classical papers [22]. There space-time is compactified on a sphere by requiring the gauge fields to approach a pure gauge at infinity. The case of QED₂ on a (continuous) torus is discussed in [23]. In both cases one can define the topological charge (Pontryagin index)

$$\nu[A] = \frac{e}{2\pi} \int d^2x F_{12}(x), \quad (6)$$

which is an integer valued functional for classical (differentiable) gauge field configurations. The Atiyah Singer Index Theorem relates the topological charge to the index of the Dirac operator, which is given by the difference of the number of positive (n_+) and negative (n_-) chirality zero modes. The zero modes are eigenstates of the Dirac operator

$$i\mathcal{D}\psi(x) = i\gamma_\mu [\partial_\mu - ieA_\mu(x)] \psi(x) = E\psi(x),$$

with eigenvalue $E = 0$. Since γ_3 anticommutes with $i\mathcal{D}$, the zero modes can be chosen as eigenstates ψ_+, ψ_- of γ_3 with $\gamma_3\psi_+ = +\psi_+$ and $\gamma_3\psi_- = -\psi_-$. n_+ (n_-) denotes the number of independent states ψ_+ (ψ_-). The Atiyah Singer Index Theorem [5] then reads

$$\nu[A] = n_+ - n_- \quad . \quad (7)$$

For the case of QED₂ there holds another index theorem, which is sometimes referred to as Vanishing Theorem [22].

$$\nu[A] > 0 \quad \implies \quad n_- = 0,$$

$$\nu[A] < 0 \quad \Longrightarrow \quad n_+ = 0 . \quad (8)$$

The Vanishing Theorem thus states that for non-zero topological charge either only positive or only negative chirality eigenmodes exist.

When computing the topological charge for the lattice gauge fields, we use the geometric definition which is based on Lüscher's idea of associating a principal bundle to each lattice configuration and defining its topological charge through the topological charge of the bundle [13]. The case of QED₂ was worked out in [24]. One obtains

$$\nu_l[U] = \frac{1}{2\pi} \sum_{x \in \Lambda} \theta_P(x) \in \mathbb{Z} . \quad (9)$$

The plaquette angle $\theta_P(x)$ is introduced as (compare (2))

$$\theta_P(x) = \text{Im} \ln U_P(x) , \quad (10)$$

and restricted to the principal branch $\theta_P(x) \in (-\pi, \pi)$. Note that configurations where $U_P(x) = -1$ for some x are so-called exceptional configurations and Lüscher's definition does not assign a value $\nu_l[U]$ to them. (This notation should not be confused with the widely used terminology where one calls exceptional configurations those gauge field configurations with bad convergence properties in the inversion algorithm for the Dirac operator.) However, those configurations are of measure zero in the path integral.

3 Analytic results for the eigensystem of the fermion matrix

This section is devoted to some analytic results on the general structure of the spectrum and the chiral properties of the eigenvectors of the fermion matrix. These results are valuable tools for our later numerical investigation of the spectrum and are necessary for a proper interpretation of an eventual approximation of the continuum index theorems by the lattice model.

3.1 The general structure of the spectrum

In this subsection we collect analytic results (*S1 - S4*) for the spectrum of the fermion matrix M which partly can be found in the literature [8, 9, 25]. Here we carefully distinguish between even and odd values of L since the structure of the spectrum changes according to L even or odd. A proper investigation of this fact is necessary for understanding an eventual realization of the index theorems (7), (8) on the lattice.

We start with noting that the hopping matrix Q , defined in (4) is similar to its hermitian adjoint Q^\dagger

$$\Gamma_3 Q \Gamma_3 = Q^\dagger, \quad (11)$$

where

$$\Gamma_3 = \mathbb{1}_{sites} \otimes \gamma_3 \quad \text{with} \quad \Gamma_3^2 = \mathbb{1}, \quad \Gamma_3^\dagger = \Gamma_3. \quad (12)$$

This implies that α is a simultaneous eigenvalue of Q^\dagger (eigenvector v), and of Q (eigenvector $\Gamma_3 v$). Let λ be some eigenvalue of Q ; then from general theorems $\bar{\lambda}$ is an eigenvalue of Q^\dagger and thus also of Q .

S1: Eigenvalues of Q and hence also of M (compare (4)) are either real or come in complex conjugate pairs.

Furthermore for L even Q is also similar to $-Q$

$$\Xi Q \Xi = -Q, \quad (13)$$

where

$$\Xi(x, y) = (-1)^{x_1+x_2} \delta_{x_1, y_1} \delta_{x_2, y_2} \otimes \mathbb{1}_{spinor} \quad \text{with} \quad \Xi^2 = \mathbb{1}, \quad \Xi^\dagger = \Xi. \quad (14)$$

For L odd (13) does not hold, since the crucial condition (compare (5))

$$\Delta_{x \pm \hat{\mu}, y} (-1)^{x_1+x_2+y_1+y_2} = -\Delta_{x \pm \hat{\mu}, y},$$

is violated for $x_\mu = 1$ (or L). The property $\Xi^2 = \mathbb{1}$ implies that if λ is an eigenvalue of Q with eigenvector v , then also $-\lambda$ is an eigenvalue of Q (eigenvector Ξv). Thus the spectrum obeys:

S2: For even L , eigenvalues of Q come in pairs $\lambda, -\lambda$.

Let us now turn to the eigenvalues μ of the fermion matrix M itself. From (4) one finds:

S3: The eigenvalues μ of the fermion matrix M are related to the eigenvalues λ of the hopping matrix Q through $\mu = 1 - \kappa\lambda$.

This has the direct consequence that for any positive, real λ there is a κ_0 such that on that gauge field configuration $\mu(\kappa_0) = 0$.

By establishing a bound on the norm of Q , further information on the spectrum can be obtained. With (4), using the fact that $1 + \gamma_\nu$ and $1 - \gamma_\nu$ are proportional to orthogonal projectors and $|U_\nu(x)| = 1$ it is straightforward to show

$$\|Q_\nu\|_\infty = \sup_g \frac{\|Q_\nu g\|}{\|g\|} = 2.$$

The norm $\|.. \|$ is defined to be the l^2 norm obtained by summing over all lattice and spinor indices and g is some (spinor) test function on the lattice. This implies for an eigenvalue λ of Q with eigenvector v

$$|\lambda| = \frac{\|Qv\|}{\|v\|} \leq \|Q\|_\infty = \|Q_1 + Q_2\|_\infty \leq \|Q_1\|_\infty + \|Q_2\|_\infty = 4.$$

Together with *S3* one finds:

S4: The eigenvalues μ of M are distributed inside a circle with radius $= 4\kappa$ with center 1 in the complex plane.

The results *S1 - S4* have important implications for an approximate realization of the index theorems (7), (8) on the lattice. For example a configuration with $|\nu_l[U]| = 1$ lets one expect (due to (7) and (8)) exactly one approximate zero-mode, i.e. exactly one eigenvalue of M with small modulus. This eigenvalue is then necessarily real, since if the lowest lying eigenvalue was complex, both this eigenvalue and its complex conjugate would have the same absolute value. The emergence of one small and real eigenvalue should be invariant under small deformations of the background field U . Finally we remark, that *S4* implies that for $\kappa < 1/4$ (which corresponds to bare mass $m > 0$) exactly vanishing eigenvalues are excluded, and real eigenvalues are positive. This corresponds to the fact that for non-vanishing quark masses m also in the continuum exact zero modes are excluded.

3.2 Chiral properties of the eigenvectors

In this section we prove a theorem on the chiral properties of the eigenvectors of the fermion matrix. It establishes that indeed, as already conjectured in the end of the last paragraph, only the eigenvectors with real eigenvalues can be interpreted as approximate zero modes.

In the continuum the zero modes can be chosen as chiral eigenstates, since γ_3 anticommutes with the Dirac operator. On the lattice the Wilson-Dirac operator has terms that explicitly break the chiral invariance and it does not anticommute any longer with γ_3 . However, it is interesting to study the pseudoscalar density matrix

$$\chi(i, j) = (v_i, \Gamma_3 v_j) \equiv v_i^\dagger \Gamma_3 v_j, \quad (15)$$

where v_i, v_j are the right eigenvectors of the hopping matrix Q with eigenvalues λ_i, λ_j . Due to (3) v_i, v_j are also eigenvectors of the fermion matrix M , with eigenvalues μ_i, μ_j related to λ_i, λ_j through $S3$. Since Γ_3 is hermitian, we find

$$\chi(j, i) = \overline{\chi(i, j)} \quad \text{and} \quad \chi(i, i) \in \mathbf{R}, \quad (16)$$

which shows that χ is a hermitian matrix. The following theorem holds:

Theorem 1 (Vanishing entries of the chiral density matrix):

$$\lambda_i \neq \overline{\lambda_j} \Rightarrow \chi(i, j) = 0, \quad (17)$$

and in particular for the diagonal elements

$$\lambda_i \notin \mathbf{R} \Rightarrow \chi(i, i) = 0. \quad (18)$$

Note that using $S3$ the conditions $\lambda_i \neq \overline{\lambda_j}$ and $\lambda_i \notin \mathbf{R}$ can immediately be written into conditions $\mu_i \neq \overline{\mu_j}$ and $\mu_i \notin \mathbf{R}$ for the eigenvalues μ_i of the fermion matrix M .

Proof: We define the matrix $H = \Gamma_3 Q$. From (11) it follows that H is hermitian and thus $(v, Hv) \in \mathbf{R}$ for arbitrary vectors v . It follows (make use of the eigenvalue equation $Qv_i = \lambda_i v_i$)

$$\mathbf{R} \ni (v_i, Hv_i) = (v_i, \Gamma_3 Qv_i) = \lambda_i (v_i, \Gamma_3 v_i) = \lambda_i \chi(i, i).$$

Since $\chi(i, i) \in \mathbf{R}$ we conclude that whenever $\chi(i, i)$ is non-vanishing, λ_i has to be real. This proves (18) for the diagonal elements. The result for the diagonal entries of the pseudoscalar density matrix may be found in [27]. Next consider

$$\begin{aligned} \mathbf{R} \ni (v_i + v_j, H[v_i + v_j]) &= \lambda_i \chi(i, i) + \lambda_j \chi(j, j) + \lambda_i \chi(j, i) + \lambda_j \chi(i, j) , \\ \mathbf{R} \ni (v_i + iv_j, H[v_i + iv_j]) &= \lambda_i \chi(i, i) + \lambda_j \chi(j, j) - i\lambda_i \chi(j, i) + i\lambda_j \chi(i, j). \end{aligned}$$

Since we already showed that the first two terms on the right hand sides are real (either λ_i is real or $\chi(i, i)$ vanishes) the last equation implies (use (16))

$$\begin{aligned} \lambda_i \overline{\chi(i, j)} + \lambda_j \chi(i, j) &\in \mathbf{R} , \\ -i\lambda_i \overline{\chi(i, j)} + i\lambda_j \chi(i, j) &\in \mathbf{R} . \end{aligned} \quad (19)$$

Introducing the abbreviations $\chi(i, j) = a + ib$, $\lambda_i = x_i + iy_i$ and $\lambda_j = x_j + iy_j$ the vanishing of the imaginary part in (19) can be expressed as

$$\begin{bmatrix} b & a \\ -a & b \end{bmatrix} \begin{bmatrix} x_i - x_j \\ y_i + y_j \end{bmatrix} = \begin{bmatrix} 0 \\ 0 \end{bmatrix} .$$

The matrix on the left has determinant $a^2 + b^2$. A non-trivial solution for the vector $(x_i - x_j, y_i + y_j)^T$ is possible only if this determinant vanishes. This implies that whenever $a^2 + b^2 \neq 0$, we must have

$$x_i = x_j , \quad y_i = -y_j \quad \Leftrightarrow \quad \lambda_i = \overline{\lambda_j} .$$

The condition $a^2 + b^2 \neq 0$ is equivalent to $\chi(i, j) \neq 0$ and thus (17) is proven. \square

Theorem 1 has important consequences for an eventual interpretation of eigenvectors of the fermion matrix as candidates for approximate zero modes. In particular the statement (18) on the diagonal entries $\chi(i, i)$ of the pseudoscalar density matrix shows that only eigenvectors v_i with *real* eigenvalues μ_i allow for non-trivial chiral properties. If one assumes that the index theorem of the continuum can be recovered from the continuum limit on the lattice, eigenvectors $v_{complex}$ with (truly) complex eigenvalues are already ruled out as candidates for zero modes, since they always obey $(v_{complex}, \Gamma_3 v_{complex}) = 0$, whereas normalized zero modes in the continuum obey $(\psi, \gamma_3 \psi) = \pm 1$.

4 Numerical results for the eigensystem of the fermion matrix

In Section 3 we explored some general aspects of the spectrum and the chiral properties of the eigenstates of the fermion matrix using analytic methods. Here we numerically analyze the behaviour of the spectrum in Monte Carlo generated background configurations.

4.1 Spectrum in fixed background configurations

In this subsection we discuss the spectrum of the fermion matrix using several *fixed* background configurations. We formulate some conjectures on the general structure of the spectrum, which will be tested in subsequent sections using the whole Monte Carlo ensemble of configurations.

When the couplings approach their critical values (compare Section 2.2) we find [28] that the physical signature (spectrum of triplet and singlet currents, chiral condensates) of the lattice model is in agreement with the continuum results for QED₂ with *massless* fermions. Thus we expect that the eigenvalues of the full fermion matrix (including the constant term) resembles the spectrum of the *massless* continuum Dirac operator. We remark that we restrict ourselves to lattices $L \times L$ with even L in order to be able to use the maximal symmetry including $S2$.

In Figures 1.a - 1.f we show the spectrum of the hopping matrix Q for a set of ‘typical’ background configurations with various values of ν_l (compare also [10, 11]). The Monte Carlo generated configurations are in equilibrium for the corresponding values of κ and β . The values of κ were chosen near the critical κ for the corresponding β .

It is obvious that all spectra obey the symmetry properties $S1$, $S2$, $S4$. The eigenvalues are either real or come in complex conjugate pairs, they are enclosed in a circle of radius 4 around the origin in the complex plane. Their distribution is symmetric with respect to reflection at the imaginary axis, as expected from $S2$ for even L .

We remark, that due to $S3$ the largest real eigenvalues of Q are to become the smallest real eigenvalues of M and thus are the candidates for the approximate zero modes. The spectra for topological charge $\nu_l = 1$ (Figs.

1.b and 1.e) show one large real eigenvalue of Q (corresponding to one small real eigenvalue of M) as was predicted already in the discussion at the end of Section 3.1. This eigenvalue has the clear interpretation of corresponding to an approximate zero mode.

In the sector with $\nu_l = 2$ (Fig. 1.c) the situation is more involved. The spacing of the two largest real eigenvalues is of similar size as their distance from the nearest pair of complex eigenvalues. Thus the size of the corresponding eigenvalues of M is *not* a proper criterion to identify them as approximate zero modes. However from the analysis of the chiral properties of the eigenvectors in Theorem 1 it is clear that the 2 small real eigenvalues of M correspond to the approximate zero modes.

It is interesting to note, that in all plots the number of real eigenvalues is equal to $4|\nu_l|$. It is generally believed [9, 10, 11] that the smaller real eigenvalues are the ‘would be’ zero modes from the doublers, which are shifted to higher values by the Wilson term. Thus one is tempted to conjecture (for L even)

$$\# \text{ of real eigenvalues} = 4|\nu_l|. \quad (20)$$

However, it has to be remarked, that (20) cannot be exact for arbitrary gauge field configurations. A counter example is given by

$$U_2(x_1, L) = -1 \quad \forall x_1 = 1, \dots, L \quad ; \quad \text{all other } U_\mu(x_1, x_2) = 1. \quad (21)$$

This configuration has $U_P(x) = 1$ for all $x \in \Lambda$ and thus $\nu_l[U] = 0$. It furthermore reduces the fermion matrix to the case of free fermions with periodic boundary conditions. The spectrum for this case can be computed using Fourier transform and is given by ($n_1, n_2 = 1, \dots, L$)

$$1 - 2\kappa \left(\cos\left(\frac{2\pi n_1}{L}\right) + \cos\left(\frac{2\pi n_2}{L}\right) \pm i\sqrt{2 - \cos^2\left(\frac{2\pi n_1}{L}\right) - \cos^2\left(\frac{2\pi n_2}{L}\right)} \right).$$

It is obvious that the imaginary parts vanish whenever $n_1, n_2 \in \{L/2, L\}$. This establishes the fact that there are real eigenvalues although $\nu_l[U] = 0$, implying that (20) can be violated for certain configurations. This possible violation was also confirmed, when we performed a numerical analysis of the spectrum for randomly chosen background configurations. In this study with static background configurations it also turned out, that the smoother the gauge field, i.e. plaquette variables close to 1, was chosen, the less likely a

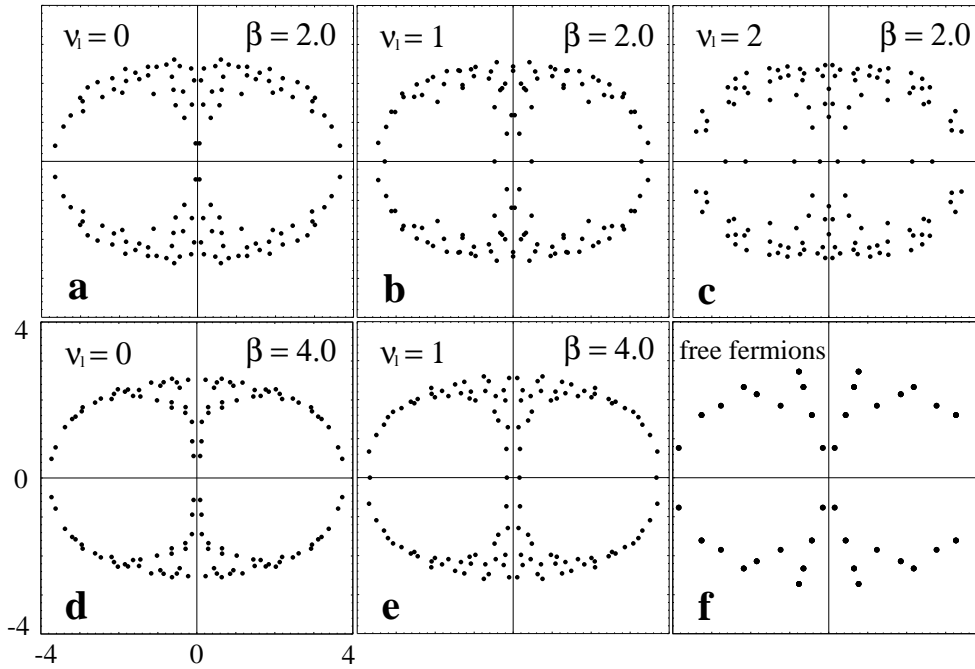


Figure 1: Spectrum of Q in the complex plane for a 8×8 lattice. The background configurations in (a-c) were taken at $\beta = 2.0$ and $\kappa = 0.276$. Plots (a), (b) and (c) correspond to $\nu_l = 0, 1$ and 2 , respectively. The parameters for (d) and (e) are $\beta = 4.0$, $\kappa = 0.262$, with (d) and (e) showing $\nu_l = 0$ and 1 . Finally in (f) we plot the spectrum, for $U = 1$, $\kappa = 0.25$ which corresponds to free massless fermions (note that we use mixed periodic boundary conditions and that the eigenvalues in (f) are degenerate).

violation of (20) became (although isolated configurations such as (21) with all plaquette variables equal 1 still violate (20)). We conjecture that up to isolated configurations, (20) is indeed correct for sufficiently smooth gauge field configurations (compare [8, 10, 11]).

4.2 The relation between the topological charge and the real eigenvalues

In the last section it was conjectured, that (20) should become correct for gauge field configurations which are smooth in some sense. In particular one is interested in the behaviour at large β since one wants to construct the continuum limit when $\beta \rightarrow \infty$. It is known that with increasing β the gauge field becomes smoother (plaquette variables closer to 1) since local fluctuations are stronger suppressed by the action.

In order to test the conjecture that the probability $p(\beta)$ of finding (20) correct increases with β , we plot $p(\beta)$ in Fig. 2 as a function of β for various lattice sizes ($L = 4, 8, 12$, and 16). For each β the value of κ was always taken to be approximately κ_{crit} for this β and lattice size, as discussed in Sec. 2.2. The values of β are 0.1, 0.5, 1.0, 1.5, 2.0, 3.0, 4.0, 5.0. For $L = 4$ and 8 we used 10^4 configurations and 10^3 for $L = 12$ and 16 .

The figure shows clearly, that already for modestly high values of β , the configurations obeying (20) entirely dominate the path integral. For $\beta > 3$, $p(\beta)$ is essentially equal to 1 for all lattice sizes we analyzed. We remark, that we found only a weak dependence of $p(\beta)$ on κ .

What is interesting to note is the difference between the various lattice sizes. For fixed $\beta < 3$ the larger lattices lag behind smaller ones in obeying (20). This poses an interesting question: Do the curves for $p(\beta)$ reach a limiting curve when L increases? Ideally when performing the continuum limit one would first like to send $L \rightarrow \infty$ followed by the limit $\beta \rightarrow \infty$. If a limiting curve with $p(\beta) = 1$ for all β larger than some finite bound β_0 emerges one could work with (20) for all $\beta > \beta_0$, independent of the lattice size. If no such limiting curve emerges, the bound $\beta_0(L)$ depends on L . However, for fixed L we can use (20) for sufficiently large β .

There is a second detail which deserves discussion, but is peculiar for QED₂. Although the classical index theorems (7), (8) are used only as a

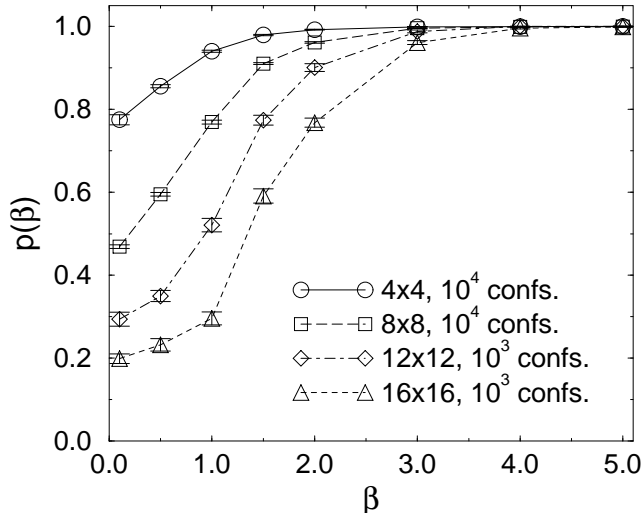


Figure 2: Probability $p(\beta)$ of finding (20) correct as a function of β . We show our results for lattice sizes $L = 4, 8, 12$ and 16 . The symbols are connected to guide the eye.

guideline in our decomposition of the path integral, the distinct role of the trivial sector in the Vanishing Theorem (8) (which only holds for QED_2) should be further analyzed. The theorem makes no statement on the trivial sector and only the Atiyah Singer Index Theorem (7) applies. Thus there is no immediate hint, that (20) should also hold for $\nu_l = 0$. In order to settle this issue, we show in Fig. 3 our results for $p(\beta)$ decomposed with respect to $|\nu_l|$ on a $L = 16$ lattice. The raw data for this plot are the same as in Fig. 2.

We find, that for $\beta \geq 1$ the different sectors are essentially uniform in obeying (20). In particular we find no anomaly for the trivial sector. We remark, that for larger β and higher $|\nu_l|$ it is difficult to obtain good statistics, since the higher sectors already have a considerably smaller weight in the path integral (compare Section 5.1). The observed high values of $p(\beta)$ for $\beta \leq 1$, $|\nu_l| \geq 1$ might be explained by the increase of the effective action with $|\nu_l|$ (see Section 5.1). Increased values of the effective action for higher $|\nu_l|$ damp additional quantum fluctuations of the gauge field in the higher sectors leading to smoother configurations with enhanced $p(\beta)$. When β increases, the configurations are forced to be smoother also in the lower sectors leading to the observed uniform behaviour in $|\nu_l|$ for higher β .

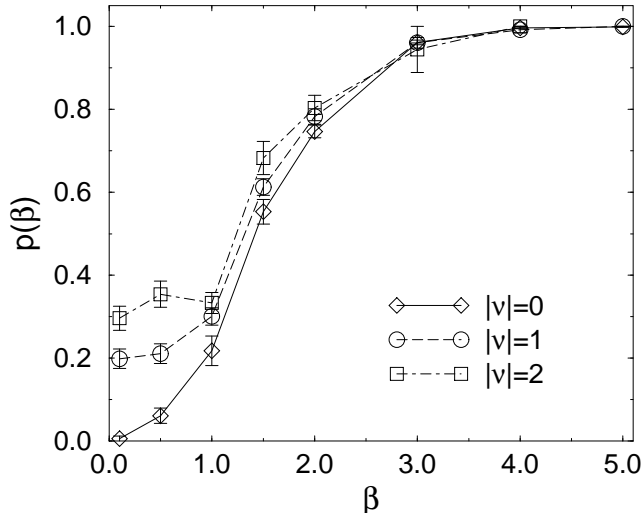


Figure 3: $p(\beta)$ decomposed with respect to $|\nu_i|$. The data were computed from the configurations on a 16×16 lattice already used in Fig. 2. The symbols are connected to guide the eye.

4.3 Properties of the spectrum in ensembles of background configurations

Pursuing the program outlined in the introduction one would like to go over from individual background configurations to an investigation of the behaviour of the spectrum in a whole ensemble of configurations with fixed winding number. In this section we establish some properties of the average behaviour of the spectrum in the ensemble of the path integral. In particular we concentrate on the real eigenvalues which are intimately connected to the topological charge, as established in the last section.

We start with showing a schematic picture (Fig. 4) for the distribution of the *real* eigenvalues of the hopping matrix Q .

The pattern displayed in Fig. 4 emerges clearly for smooth configurations and becomes more pronounced for increasing values of β (see also [10]). We find that the real eigenvalues are concentrated in the small domains A, B, A^* and B^* . The eigenvalues in A are related to the eigenvalues in A^* through the symmetry $\lambda \leftrightarrow -\lambda$ ($S2$) and the same holds for B and B^* . We find that

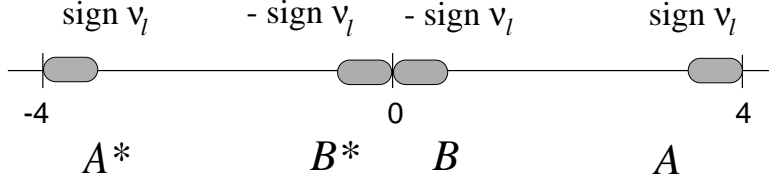


Figure 4: Schematic picture of the distribution of the real eigenvalues of the hopping matrix Q . The shaded areas are the domains A^* , B^* , B and A where the real eigenvalues concentrate. In the top line we indicate how the sign of the matrix elements $\chi(i, i)$ corresponding to the eigenvalues in the domains is related to the sign of the topological charge ν_l .

the corresponding diagonal entries of the pseudoscalar density matrix $\chi(i, i)$ are equal (as a matter of fact this can be proven analytically, using similar techniques as in the proof of Theorem 1). Also the sign of the diagonal entries obeys a simple pattern: It coincides with the sign of ν_l for the regions A, A^* and equals minus the sign of ν_l for B and B^* . This shows that the eigenvectors corresponding to domain A , which are the approximate zero modes (their eigenvalues of M approach 0) also have the correct chirality as expected from (7), (8).

We find that with increasing β the domains A and B shrink and are shifted towards the limiting values 4 and 0 respectively (see also [10, 11]). In order to quantify this statement, we computed the average values \bar{A}, \bar{B} and the standard deviations σ_A, σ_B of the real eigenvalues in each of the domains A and B . The eigenvalues can be attributed to A or B due to the chiral properties of the eigenvectors (i.e. the sign of $\chi(i, i)$).

Fig. 5.a shows our results for 8×8 lattices and various values of β . For $\beta \leq 2$ we evaluated 10^4 configurations in non-trivial sectors, for $\beta = 3, 4, 5$ we used 10^3 nontrivial configurations. The symbols give the average values \bar{A} (diamonds) and \bar{B} (squares) of the real eigenvalues in A, B . horizontal bars show the corresponding standard deviations σ_A, σ_B . Note that this is not some kind of errorbar giving the size of statistical errors, but gives the average size of the regions A and B . It is obvious, that with increasing β the real eigenvalues get confined in smaller regions closer to the limits 0 and 4.

The same picture also holds for each sector separately. In Fig. 5.b we show the same quantities as in Fig. 5.a, but restrict the ensemble to configurations

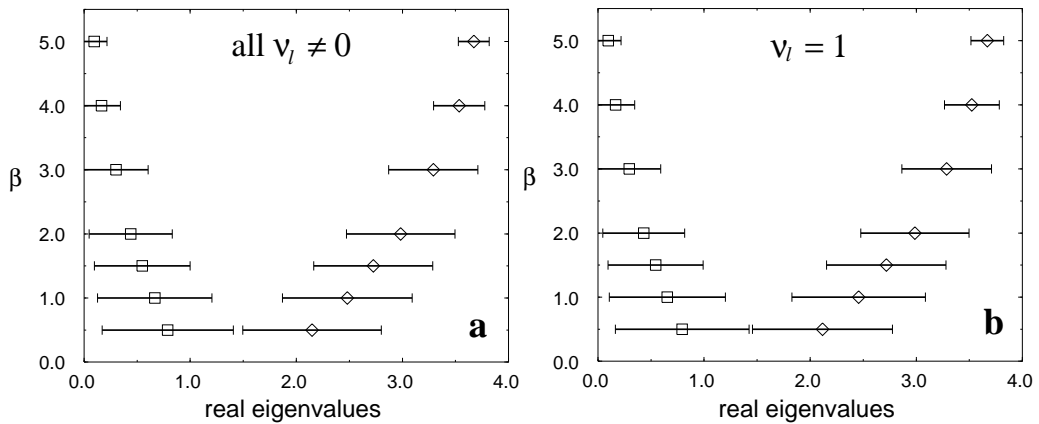


Figure 5: Average behaviour of the distribution of the real eigenvalues for various values of β . The data were taken on a 8×8 lattice (see the text for statistics). Fig. 5.a (left-hand plot) shows the average values \bar{A}, \bar{B} of the real eigenvalues in the domains A (diamonds, right branch) and B (squares, left branch). The horizontal bars show the size of the standard deviations σ_A, σ_B from the average values. We stress that this is not a statistical error, but gives the average size of the domains A and B . In Fig. 5.b (right-hand plot) we show the same information but take into account only configurations with $\nu_l = 1$.

with $\nu_l = 1$. Again we find that with increasing β the real eigenvalues get confined in smaller regions closer to the limits 0 and 4.

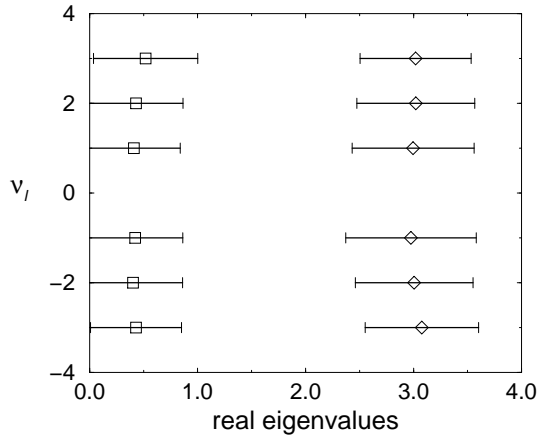


Figure 6: Average behaviour of the distribution of the real eigenvalues for different ν_l . The data were computed from 2300 configurations in non-trivial sectors on a 16×16 lattice at $\beta = 2, \kappa = 0.276$. The symbols give the average values $\overline{A}, \overline{B}$ of the real eigenvalues in A (diamonds, right-hand branch) and B (squares, left-hand branch). The horizontal bars are the corresponding standard deviations σ_A, σ_B .

If one compares the different topological sectors (β fixed) one finds that the average values $\overline{A}, \overline{B}$ of the real eigenvalues in A, B are rather independent of ν_l and also the size of the domains A, B is rather invariant. This is demonstrated in Fig. 6 where we show average value and standard deviation of the eigenvalues in A and B as a function of the topological charge. We used 2300 configurations in non-trivial sectors, generated on a 16×16 lattice at $\beta = 2, \kappa = 0.276$ ($\approx \kappa_{crit}$).

Also the diagonal entries $\chi(i, i)$ of the pseudoscalar density matrix show a simple behaviour, monotone in β . We computed the average values $\overline{\chi_A}, \overline{\chi_B}$ of the $\chi(i, i)$ and their standard deviation σ_χ from this value for each domain A, B separately. Fig. 7 shows our result for the same sample used in Fig. 5.b. ν_l is positive ($=1$), and as expected from (7) and (8) domain A (diamonds) has positive $\chi(i, i)$, while in region B (squares) we find negative values. Both branches show a clear trend towards the continuum values -1 and 1 with increasing β . Also the interval containing $\chi(i, i)$ (horizontal bars) shrinks for

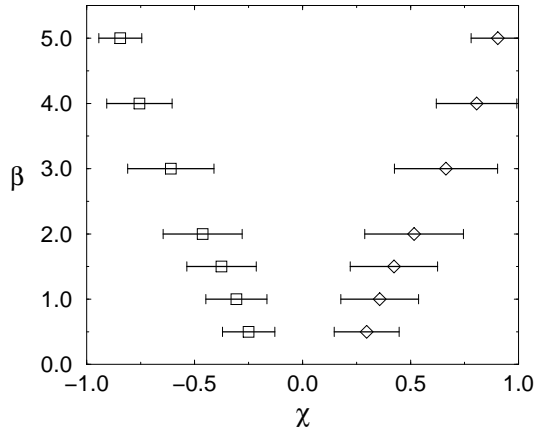


Figure 7: Average values $\overline{\chi}_A, \overline{\chi}_B$ of the entries $\chi(i, i)$ of the pseudoscalar density matrix corresponding to eigenvalues in A (diamonds, right branch) and B (squares, left branch) in the $\nu_l = 1$ sector. The horizontal bars show the size of the standard deviation σ_χ from the average value. The data were computed from the same configurations used in Fig. 5.

larger β .

We summarize the emerging picture for the structure of the spectrum in the ensemble of the path integral as follows (L is even):

E1: Only real eigenvalues can correspond to approximate zero modes, since for complex eigenvalues the diagonal entries of the pseudoscalar density matrix vanish identically (Theorem 1).

E2: For large β the path integral is entirely dominated by configurations obeying $\#$ of real eigenvalues = $4|\nu_l|$ (Fig. 2).

E3: The real eigenvalues group according to the scheme depicted in Fig. 4. The domains A, B, A^, B^* are related through $S2$ and the doubler symmetry.*

E4: With increasing β the domains A and B shrink and move towards the limiting values 4 and 0 (Fig. 5).

E5: The sign of the diagonal entries $\chi(i, i)$ of the pseudoscalar density matrix coincides with the sign of ν_l for the eigenvalues in A, A^ (as expected from*

(7), (8)) and is minus this sign for B, B^* . With increasing β , the values of $\chi(i, i)$ get confined in shrinking regions approaching the limiting values ± 1 (Fig. 7).

E6: The behaviour of the eigensystem is essentially uniform in ν_l (Figures 3 and 6).

In the remaining sections we use these results for analyzing the contribution of different topological sectors to the path integral and to vacuum expectation values of various operators.

5 Applications

In this section we bring in the harvest from the previous investigation of the interplay between topological charge and behaviour of the spectrum of the fermion matrix. We will demonstrate, that the analytic results *S1 - S4* and Theorem 1, together with the results *E1 - E6* on the spectrum in ensembles of background configurations provide a powerful tool for analyzing physical questions in lattice gauge theory. Here we concentrate on local and bulk quantities. The study of the dependence of the spectrum (which requires the computationally more demanding analysis of two-point functions (see also [26])) on the topological charge is reserved for a forthcoming publication [28].

5.1 Effective action and fermion determinant

In this first application we concentrate on the behaviour of the effective action and in particular of the fermion determinant in the various sectors.

After integrating out the fermions (note that we use 2 explicit flavors of fermions (not to be mixed up with the doublers implicit in the Wilson action) one obtains the effective action for the gauge fields

$$S^{eff}[U] = S_g[U] + S_f^{eff}[U] = S_g[U] - \ln \det M[U]^2. \quad (22)$$

It is interesting to analyze typical values of the effective action in various topological sectors. For the gauge field part of the action it is known [29], that there exist lower bounds of the action for each sector. In a previous

article [30] we analyzed the role of these bounds in the case of pure $U(1)_2$ gauge theory on the lattice (we will comment on this below). Due to the relation of topological charge and zero modes via the index theorems, also the fermion determinant depends on the topological sectors in a non-trivial way.

In Fig. 8 we show our results for the averages of the gauge field action $\overline{S}_g(\nu)$ and the effective action from the fermions $\overline{S}_f^{eff}(\nu)$ in each of the sectors. We give the results per plaquette, i.e. normalized with L^{-2} .

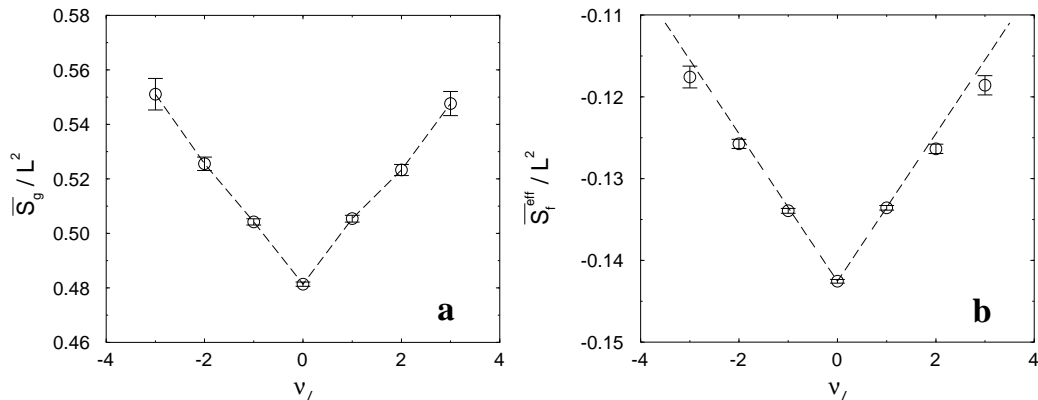


Figure 8: Average value of the contributions of the gauge field action $\overline{S}_g(\nu_l)/L^2$ ((a) left-hand side) and of the fermions $\overline{S}_f^{eff}(\nu_l)/L^2$ ((b) right-hand side) to the effective action. The average was taken for each topological sector separately. The data were obtained from a simulation on a 16×16 lattice at $\beta = 2, \kappa = 0.276$ using 10^4 configurations. In (a) we connect the symbols to guide the eye. The straight line in (b) was drawn using (27) below.

Fig. 8.a (left-hand plot) shows the average value $\overline{S}_g(\nu)$ of the gauge field action in each topological sector separately. We find a behaviour which is essentially linear in $|\nu_l|$. If one compares this result with the pure gauge theory [30] the linear behaviour is rather surprising. In the quenched case we found a behaviour of the gauge field action which is quadratic in ν_l with a variation in ν_l which is of one order of magnitude smaller than here. This result was understood in a quantitative way using an argument based on the topology of the configurations [30]. The essentially linear behaviour (plus eventually a small quadratic term) in Fig. 8.a has no such simple explanation.

In the unquenched model it is not the gauge field action alone which is minimized, but the effective action (22) which is the sum of the gauge field action and the contribution from the fermion determinant. Obviously the influence of the fermions adds a linear term which entirely changes the picture of the pure gauge theory. The interplay of the two terms in (22) does not allow for a simple topological explanation as in [30].

There is however a lesson from the study of the pure gauge theory [30] which is also confirmed in the unquenched model: The lower bounds for the action in each topological sector are at least one order of magnitude smaller than the average value of the gauge field action. We also computed the distribution of the values of the action, and find that quantum fluctuations keep most of the configurations high above the lower bounds in each sector [30]. The same observation is true for the model with fermions. This is in particular remarkable, since the lower bounds given in [30] are saturated by classical configurations with constant electric field, carrying topological charge. The path integral for the Schwinger model on the torus including all topological sectors can be constructed by dressing these classical configurations with quantum fluctuations [23]. The observed high values of the gauge field action for the main part of the configurations is a demonstration of the importance of quantum fluctuations (see [30] for a more detailed discussion).

Fig. 8.b (right-hand plot) shows the average value $\overline{S}_f^{eff}(\nu_l)/L^2$ of the contribution of the fermions to the effective action for each topological sector. Again we find a behaviour essentially linear in $|\nu_l|$. This behaviour can be understood in a quantitative way using the results from the previous sections, as will be shown now.

From $S2$, $S3$ it follows (L even) that real eigenvalues ρ of M come in pairs

$$\rho^{(1)} = 1 - \kappa w \quad , \quad \rho^{(2)} = 1 + \kappa w \quad , \quad (23)$$

with $0 \leq w \leq 4$. $E2$ and $E3$ establish, that for large enough β

$$\# \text{ of real pairs} = 2|\nu_l| \quad , \quad (24)$$

and that the real pairs are equally distributed among the domains $A \cup A^*$ and $B \cup B^*$. The determinant of M is the product of all eigenvalues. For the contribution of the real pair (23) one obtains

$$R = \rho^{(1)} \rho^{(2)} = 1 - (\kappa w)^2 \quad . \quad (25)$$

In *E4* we establish, that the regions A and B (and of course also their $S2$ images A^* and B^*) shrink and approach their limiting values 0 and ± 4). Thus we obtain characteristic contributions from the real eigenvalues in $A \cup A^*$ and $B \cup B^*$ described by the average values \overline{A} , \overline{B}

$$R_A = 1 - (\kappa \overline{A})^2 \quad , \quad R_B = 1 - (\kappa \overline{B})^2 . \quad (26)$$

The contribution of the complex eigenvalues is more difficult to handle. However by inspecting the spectra for several configurations (see Fig. 1 for a few examples) we find that whenever $|\nu_l|$ increases by one unit, one of the complex quadruplets vanishes and is turned into two real pairs. The rest of the complex eigenvalues remains rather unperturbed giving some positive (note that complex eigenvalues come in complex conjugate pairs) constant c . As long as $|\nu_l|$ is considerably smaller than the overall amount of eigenvalues $2L^2$, we make the following ansatz for the contribution of the fermion determinant to the effective action:

$$S_f^{eff} = -\ln \det(M)^2 \simeq -\ln \left(c(R_A R_B)^{|\nu_l|} \right)^2 = C - |\nu_l| 2 \ln |R_A R_B| . \quad (27)$$

The expression gives a behaviour linear in $|\nu_l|$ and predicts also the slope of the line. The constant term has to be taken from the numerical data. Evaluating 2300 configurations for these parameters ($L = 16, \beta = 2, \kappa = 0.276$) we obtained $\overline{A} = 2.996(8)$, $\overline{B} = 0.421(7)$. The straight line in Fig. 8.b was drawn using (27) with these numbers. We find good agreement with the Monte Carlo data. Eq. (27) slightly overestimates the Monte Carlo results for larger $|\nu_l|$. This might be due to the fact that by increasing $|\nu_l|$ by one, four new real eigenvalues emerge causing one complex quadruplet to vanish. Thus the contribution from the complex eigenvalues is not entirely independent of $|\nu|$ as we assumed in our ansatz. This effect should become smaller with increasing L . We believe that the essentially linear relation, and the good performance of (27) shows that the behaviour of the fermion determinant as a function of ν_l can be understood from the analysis of the spectrum of the fermion matrix in Sections 3 and 4 in a quantitative way (compare also [11]).

We end this section with a remark on the positivity of the fermion determinant $\det M$. From *S1 - S3* we know that the complex eigenvalues come in

quadruplets

$$\begin{aligned}\mu^{(1)} &= 1 - \kappa (x + iy) & , & & \mu^{(2)} &= 1 - \kappa (x - iy) , \\ \mu^{(3)} &= 1 + \kappa (x + iy) & , & & \mu^{(4)} &= 1 + \kappa (x - iy) ,\end{aligned}$$

contributing a factor

$$\prod_{\alpha=1}^4 \mu^{(\alpha)} = \left[(1 - \kappa x)^2 + \kappa^2 y^2 \right] \left[(1 + \kappa x)^2 + \kappa^2 y^2 \right] ,$$

to the fermion determinant. Obviously the factor from a complex quadruplet is strictly positive.

The second order polynomial $1 - (\kappa w)^2$ which one obtains for the contribution of a pair of real eigenvalues (25) becomes negative for $\kappa w > 1$. Thus a negative value of the fermion determinant can only come from pairs of real eigenvalues. Since the emergence of real eigenvalues is connected to gauge field configurations with non vanishing topological charge (compare E2) the positivity properties of the determinant are as well. In the literature one often encounters the approximation

$$\det(M) \sim |\det(M)| ,$$

used to simulate odd numbers of flavors. This might possibly lead to a wrong weight from non-trivial topological sectors.

In order to investigate this possibility we performed several simulations on $L = 8$ lattices at $\beta = 2$. The values of κ were chosen above the critical κ (which is $\kappa_{crit} \approx 0.276$ for $\beta = 2$) in order to force the determinant to negative values. κ varied between 0.280 and 0.335. For $\kappa \geq 0.320$ we found negative values of the determinant in the non-trivial sectors. It is interesting to remark, that we then also found a considerably enhanced abundance of configurations in the higher sectors. The mechanism for this trapping is due to the contribution of the real eigenvalues to the effective fermion action, which is essentially the sum of the logarithms of the eigenvalues squared (note that we squared the determinant for the updating). Once one of the real eigenvalues assumes a negative value (thus causing the determinant to be negative), it can *continuously* go back to a positive value only by passing through zero. This however drives the logarithm and thus the effective action to infinity. The only way back is through a discontinuous jump, which

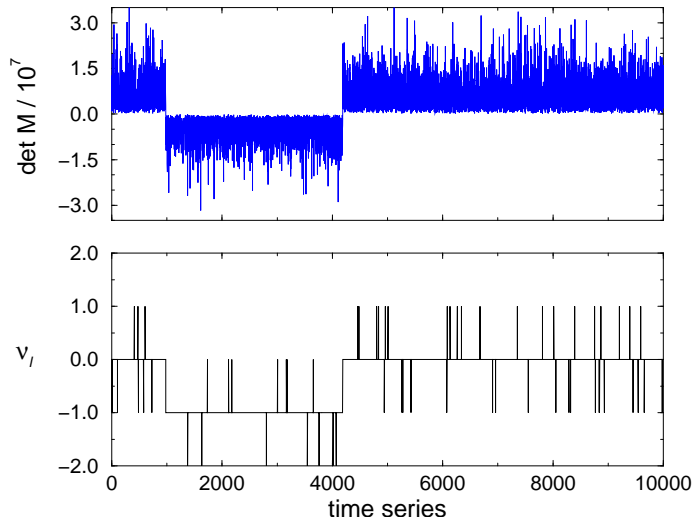


Figure 9: Time series of the fermion determinant and the topological charge.

probably costs a big amount of action. This creates a barrier, which traps the system in a topologically non-trivial sector.

Fig. 9 shows a time series for the determinant and the topological charge from 10^4 configurations at $\beta = 2$, $\kappa = 0.33$. For approximately the first 1000 configurations the topological charge is mainly zero with a few configurations that fluctuate to $\nu_l = \pm 1$. The determinant has only positive values. Then for approximately 3400 configurations, the determinant has negative values, and the topological charge is mainly trapped at $\nu_l = -1$ implying that the fermion matrix has 4 real eigenvalues (and thus can have negative values). There are a few configurations with $\nu_l = 0$ or 2. From the sign of the determinant we conclude that there still are quadruplets of real eigenvalues, although e.g. ν_l vanishes. These are just the configurations violating (20) in agreement with our observation in Fig. 2. However, the system is obviously trapped in the $\nu_l = -1$ sector for more than 3000 configurations. After that a tunneling back to positive values of the determinant occurs and the system evolves again with positive values of the determinant and the distribution of the values of ν_l is again symmetric around 0.

5.2 The pseudoscalar density

In this section we discuss the contributions of different topological sectors to the vacuum expectation value of the pseudoscalar density. This operator plays an important role in the so called ‘fermionic definition’ [6] - [9] of the topological charge which uses the chiral Ward identity to define the topological charge and is also used in the lattice derivation of the Witten-Veneziano formula [31].

Due to translation invariance, the vacuum expectation value of the pseudoscalar density can be written as

$$\langle \bar{\psi}(x)\gamma_3\psi(x) \rangle = \frac{1}{L^2} \sum_{x \in \Lambda} \langle \bar{\psi}(x)\gamma_3\psi(x) \rangle = \frac{1}{Z L^2} \int [dU] e^{-S^{eff}[U]} \text{Tr} (M^{-1}\Gamma_3). \quad (28)$$

In Fig. 10 we show our results for the average value $\overline{\text{Tr}(M^{-1}\Gamma_3)}$ in ensembles of background configurations with different ν_l ($L = 16, \beta = 2, \kappa = 0.276, 10^4$ configurations). Note that in these averages, the observable was not multiplied with the Boltzmann factor $\exp(-S^{eff}[U])$.

The Monte Carlo data show a linear behaviour in ν_l with a positive slope. Such a behaviour can already be expected from the spectral decomposition of the continuum Dirac operator in classical background configurations. The continuum operator $i\mathcal{D}$ is hermitian, implying that eigenstates to different eigenvalues are orthogonal. If ψ is an eigenstate with eigenvalue E , then due to $\{i\mathcal{D}, \gamma_3\} = 0$, $\gamma_3\psi$ has eigenvalue $-E$. Thus the matrix elements $\langle \psi | \gamma_3 | \psi \rangle$ vanish whenever ψ is not a zero mode. The only states that can contribute in the spectral decomposition of the pseudoscalar density are the zero modes. Since their number is equal to ν due to Index and Vanishing Theorem (7), (8) the linear behaviour follows for classical background configurations.

The lattice Wilson-Dirac operator is not hermitian, even worse, not normal. Thus its (right) eigenvectors do not form an *orthonormal* basis, and the continuum argument cannot be taken over to the lattice. However, we established (E1) that the real eigenvalues on the lattice take over the role of the zero eigenvalues in the continuum. We furthermore demonstrated (E2) that the number of real eigenvalues is proportional to $|\nu_l|$. Finally we found (E5) that the chiral properties (i.e. the sign of the entry in the pseudoscalar density matrix) of the real eigenvalues in the physical region A behaves as

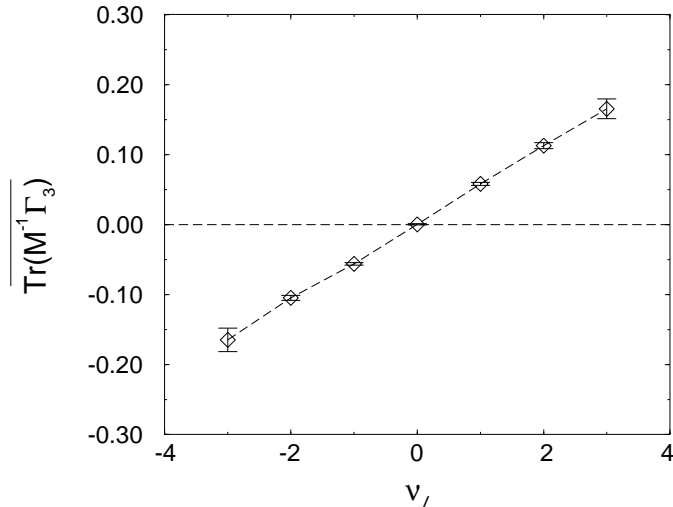


Figure 10: Average values of $\overline{\text{Tr}(M^{-1}\Gamma_3)}$ in different topological sectors. The symbols show the results from the Monte Carlo simulation ($L = 16, \beta = 2, \kappa = 0.276, 10^4$ configurations). The symbols are connected to guide the eye.

in the continuum. These three ingredients allow to understand the observed linear behaviour of the pseudoscalar density.

6 Discussion

In this study we have demonstrated, that the existence of an integer valued lattice equivalent of the topological charge has important consequences. We believe, that the use of the topological charge on the lattice goes far beyond its applications in continuum formulations of gauge theories. We have shown, that a careful analytic investigation of the spectral decomposition of the fermion matrix supports the interpretation of the real eigenvalues (and the corresponding eigenvectors) as the zero eigenvalues (zero modes) of the continuum Dirac operator. It should be stressed again, that this is a result for *all* configurations contributing in the continuum limit, while the Index Theorems in the continuum only hold for classical gauge fields. When concentrating only on the real eigenvalues (which is much less demanding than

treating the whole spectrum), numerical methods were successfully used to analyze their distribution when approaching the continuum limit. We have shown, that the results for the spectrum can be used to understand the interplay between topological charge and physical quantities in a quantitative way.

As discussed in the introduction, QED_2 has many features in common with QCD_4 . The physical picture we obtained for the 2-dimensional theory thus provides an interesting model for the 4-dimensional case. We remark, that not only the physical picture, but also some of the mathematical results we obtained may be extended to QCD_4 . In particular Theorem 1 which is the conceptual backbone of this study has a straightforward generalization to the 4-dimensional case [12].

Other aspects are certainly considerably simpler in the 2-dimensional world. In 4-dimensions and for non-abelian gauge groups, the fermion matrix has much larger dimension, and explicit diagonalization becomes a challenging enterprise [32]. However, with the identification of the real part of the spectrum as the trace of non-trivial topological charge, related physical questions might be tackled without knowing all of the spectrum. When concentrating only on the real part, computational simplifications might be possible [12].

Although from a conceptual point of view most satisfactory, the geometric definition of the topological charge is very costly to evaluate for non-abelian gauge groups. Other definitions such as the ‘fermionic approach’ using the chiral Ward identity [6] - [9] might be simpler to compute. The latter approach essentially makes use of the pseudoscalar density operator. We expect that also the results for the pseudoscalar density in Section 5.2 can be taken over to QCD_4 [12] and might lead to a considerable simplification of the fermionic ansatz for the topological charge.

Acknowledgment: We thank Philippe de Forcrand, Helmut Gausterer, Erhard Seiler, Gordon Semenoff and Renate Teppner for remarks and interesting discussions.

References

- [1] R. Jackiw and C. Rebbi, Phys. Rev. Lett. **37** (1976) 172;
C.G. Callan, R.F. Dashen and D.J. Gross, Phys. Lett. **63B** (1976) 334.
- [2] P. Colella and O.E. Lanford III, in: *Constructive Quantum Field theory* (Erice 73), G. Velo and A. Wightman (Eds.), Springer Lecture Notes in Physics, Springer 1973, New York.
- [3] A.S. Kronfeld, Nucl. Phys. **B** (Proc. Suppl.) **4** (1988) 329.
- [4] A. Di Giacomo, Nucl. Phys. (Proc. Suppl.) **B47** (1996) 136.
- [5] M. Atiyah and I.M. Singer, Ann. Math. **93** (1971) 139.
- [6] F. Karsch, E. Seiler and I.O. Stamatescu, Nucl. Phys. **B271** (1986) 349.
- [7] I. Barbour and M. Teper, Phys. Lett. **175B** (1986) 445.
- [8] J. Smit and J.C. Vink, Phys. Lett. **194B** (1987) 433; Nucl. Phys. **B286** (1987) 485; Nucl. Phys. **B303** (1988) 36;
M.L. Laursen, J. Smit and J.C. Vink, Nucl. Phys. **B343** (1990) 522.
- [9] S. Itoh, Y. Iwasaki and T. Yoshié, Phys. Rev. **D36** (1987) 527;
Phys. Lett. **184B** (1987) 375.
- [10] J.C. Vink, Nucl. Phys. **B307** (1988) 549.
- [11] W. Bardeen, A. Duncan, E. Eichten and H. Thacker, preprints hep-lat/9705002, hep-lat/9705008.
- [12] C.R. Gatttringer, I. Hip and C.B. Lang, work in preparation.
- [13] M. Lüscher, Commun. Math. Phys. **85** (1982) 39.
- [14] J. Schwinger, Phys. Rev. **128** (1962) 2425.
- [15] S. Coleman, Phys. Rev. **D11** (1975) 2088; Ann. Phys. **101** (1976) 239;
R.F. Dashen, B. Hasslacher and A. Neveu, Phys. Rev. **D11** (1975) 3424.

- [16] S. Coleman, R. Jackiw and L. Susskind, *Ann. Phys.* **93** (1975) 267;
 E. Seiler and J. Fröhlich, *Helv. Phys. Acta* **49** (1976) 889;
 C. Gatttringer, *On the U(1) Problem of QED₂*, Thesis, University of Graz, Austria 1995, preprint hep-th/9503137 (1995); *Ann. Phys.* **250** (1996) 389;
 C. Adam, *Phys. Lett.* **363B** (1995) 79; *Phys. Lett.* **382B** (1996) 383; preprint hep-th/9704064 (1997).
- [17] S. Duane, A. D. Kennedy, B. J. Pendleton and D. Roweth, *Phys. Lett.* **195B** (1987) 216.
- [18] P. de Forcrand, *Nucl. Phys. B (Proc. Suppl.)* **47** (1996) 228.
- [19] A. Frommer, V. Hannemann, Th. Lippert, B. Noeckel and K. Schilling, *Int. J. Mod. Phys.* **C5** (1995) 1073.
- [20] K. Jansen, C. Liu, M. Lüscher et al., *Phys. Lett.* **B372** (1996) 275; M. Bochicchio, L. Maiani, G. Martinelli et al., *Nucl. Phys.* **B262** (1985) 331.
- [21] I. Hip, C.B. Lang and R. Teppner, work in preparation.
- [22] J. Kiskis, *Phys. Rev.* **D15** (1977) 2329;
 N.K. Nielsen, B. Schroer, *Nucl. Phys.* **B127** (1977) 493;
 M.M. Ansourian, *Phys. Lett.* **70B** (1977) 301.
- [23] H. Joos, *Helv. Phys. Acta* **63** (1990) 670;
 I. Sachs and A. Wipf, *Helv. Phys. Acta* **65** (1992) 652.
- [24] R. Flume and D. Wyler, *Phys. Lett.* **108B** (1981) 317;
 C. Panagiotakopoulos, *Nucl. Phys.* **B251** (1985) 61;
 A. Phillips, *Ann. Phys.* **161** (1985) 399;
 M. Göckeler, A.S. Kronfeld, G. Schierholz and U.-J. Wiese, *Nucl. Phys.* **B404** (1993) 839;
 H. Gausterer and M. Sammer, preprint hep-lat/9609032 (1996).
- [25] D.H. Weingarten and J.L. Challifour, *Ann. Phys.* **123** (1979) 61.
- [26] H. Dilger, *Nucl. Phys.* **B434** (1995) 321.

- [27] R. Narayanan and H. Neuberger, Nucl. Phys. **B443** (1995) 305.
- [28] C.R. Gatttringer, I. Hip and C.B. Lang, work in preparation.
- [29] A.A. Belavin, A.M. Polyakov, A.S. Schwartz and Yu.S. Tyupkin, Phys. Lett. **59B** (1975) 85.
- [30] C.R. Gatttringer, I. Hip and C.B. Lang, preprint hep-lat/9706010, (Phys. Lett. B in print).
- [31] J. Smit and J.C. Vink, Nucl. Phys. **B284** (1987) 234.
- [32] R. Setoodeh, C.T.H. Davies and I.M. Barbour, Phys. Lett. **213B** (1988) 195;
T. Kalkreuter, Phys. Rev. **D51** (1995) 1305; Nucl. Phys. **B** (Proc. Supl.) **49** (1996) 168.